Measurements of the mass absorption cross section of atmospheric soot particles using Raman spectroscopy

S. Nordmann,[1] W. Birmili,[1] K. Weinhold,[1] K. Müller,[1] G. Spindler,[1] and A. Wiedensohler[1]

Received 12 April 2013; revised 1 October 2013; accepted 11 October 2013; published 5 November 2013.

[1] Soot particles are a major absorber of shortwave radiation in the atmosphere. The mass absorption cross section is an essential quantity to describe this light absorption process. This work presents new experimental data on the mass absorption cross section of soot particles in the troposphere over Central Europe. Mass absorption cross sections were derived as the ratio between the light absorption coefficient determined by multiangle absorption photometry (MAAP) and the soot mass concentration determined by Raman spectroscopy. The Raman method is sensitive to graphitic structures present in the particle samples and was calibrated in the laboratory using Printex®90 model particles. Mass absorption cross sections were determined for a number of seven observation sites, ranging between 3.9 and 7.4 $m^2\ g^{-1}$ depending on measurement site and observational period. The highest values were found in a continentally aged air mass in winter, where soot particles were assumed to be mainly internally mixed. Our values are in the lower range of previously reported values, possibly due to instrumental differences to the former photometer and mass measurements. Overall, a value of 5.3 $m^2\ g^{-1}$ from orthogonal regression over all samples is considered to be representative for the soot mass absorption cross section in the troposphere over Central Europe.

Citation: Nordmann, S., W. Birmili, K. Weinhold, K. Müller, G. Spindler, and A. Wiedensohler (2013), Measurements of the mass absorption cross section of atmospheric soot particles using Raman spectroscopy, *J. Geophys. Res. Atmos.*, *118*, 12,075–12,085, doi:10.1002/2013JD020021.

1. Introduction

[2] Soot particles are a product of an incomplete combustion of fossil fuels and biomass. On a global scale, soot particles emerge predominantly from man-made processes although natural sources exist as well. The largest amounts of soot from fossil fuel burning are currently emitted in industrialized countries of the northern hemisphere as a result of more or less controlled energy production processes. Biomass burning of savanna, forests, and agricultural waste dominate the soot emissions in Africa and South America [*Bond et al.*, 2004]. Soot particles are chemically rather inert with particle diameters around 100 nm being the most frequent, so that they may be transported across the globe even to the remotest regions like the Arctic [*Heintzenberg*, 1982].

[3] Soot particles are good absorbers of solar radiation. They absorb shortwave radiation across a broad spectral region and can thus thermally heat their environment. As a consequence of light absorption, soot decreases the reflectivity of the surface-atmosphere-cloud system. Deposited on snow, it may also reduce surface reflectivity. On a global scale, the direct radiative forcing of soot is positive at the top of the atmosphere and negative at the surface, leading to an overall warming effect [*Ramanathan and Carmichael*, 2008]. Moreover, if soot particles are incorporated into cloud processes, they may reduce cloud cover by heating their environment [*Ackerman et al.*, 2000], which is also designated as the semidirect effect. The Intergovernmental Panel on Climate Change (IPCC) [*Forster et al.*, 2007] summarized the positive direct radiative forcing of soot to be in the range of Methane but with a large uncertainty. Besides climate, soot has also significant effects upon human health. A recent WHO report summarizes the existing evidence of adverse health effects of black carbon including cardiopulmonary morbidity and mortality [*Janssen et al.*, 2012].

[4] The quantification of soot-related effects has suffered from the lack of a uniform definition of soot [*Baumgardner et al.*, 2012]. Several instrumental approaches are available, which make use of either the light-absorptive properties, structural characteristics, and even the volatility of soot particles [*Bond and Bergstrom*, 2006; *Andreae and Gelencsér*, 2006; *Moosmüller et al.*, 2009]. The term black carbon (BC) basically accounts for the absorptive components of soot particles. Light is absorbed, in particular, by small graphitic domains designated as graphitic carbon (GC). However, atmospheric samples may also include light-absorbing substances other than soot, which may interfere with a BC

Additional supporting information may be found in the online version of this article.

[1]Leibniz Institute for Tropospheric Research, Leipzig, Germany.

Corresponding author: S. Nordmann, Institute for Tropospheric Research, Permoserstrasse 15, 04318 Leipzig, Germany. (nordmann@tropos.de)

©2013. American Geophysical Union. All Rights Reserved.
2169-897X/13/10.1002/2013JD020021

measurement. Elemental carbon (EC) is defined as the refractory fraction of soot particles that remains, as opposed to organic carbon (OC), stable at high temperatures. The relationships between BC, GC, and EC are usually not necessarily constant and may sensitively depend on the conditions during soot formation and the further course of aging processes in the atmosphere. *Andreae and Gelencsér* [2006] summarized different definitions for atmospheric soot particles. For aggregates of spherules made of graphene layers and without organic substances, they used the symbol C_{soot}.

[5] A method particularly sensitive to GC is Raman spectroscopy. *Rosen and Novakov* [1977] unambiguously identified GC in atmospheric samples by evaluating characteristic bands in the Raman spectrum. *Keller and Heintzenberg* [1997] developed a practical method to quantify GC in atmospheric samples on polycarbonate filters by near-infrared Fourier-transform (NIR-FT) Raman spectroscopy. *Mertes et al.* [2004] applied this method to quartz fiber filters.

[6] In this work, we modified and recalibrated this method for glass microfiber filters used for BC measurements in the multiangle absorption photometer (MAAP). For calibration we used the industrial carbon black material Printex®90 which is, in the suspended state, expected to be very similar to C_{soot}. BC and C_{soot} can thus be made available as two independent parameters for the very same aerosol sample. From BC and C_{soot}, a mass absorption cross section ($\alpha_{C,soot}$) can be derived—a quantity that is often needed to calculate the radiative transfer and radiative forcing caused by soot particles. The literature values of the mass absorption cross section show a large span between 4 and 18 $m^2\ g^{-1}$ for wavelengths between 550 and 637 nm [e.g., *Carrico et al.*, 2003; *Kondo et al.*, 2009; *Hitzenberger et al.*, 2006]. It has not been clear whether this large span is a real effect of soot-related properties (e.g., mixing state) in the atmosphere or due to instrumental differences.

[7] The new Raman method for the determination of C_{soot} mass concentrations is applied on a range of atmospheric particle samples collected in the German Ultrafine Aerosol Network (GUAN). Determining $\alpha_{C,soot}$ for different measurement sites, atmospheric conditions, and states of mixing and the analysis of these effects is the prime goal of this work.

2. Experimental

2.1. General Approach

[8] This study couples experiments with artificial soot particles in the laboratory (section 3) with the analysis of atmospheric soot samples (section 4). The field measurements were made at seven sites of the German Ultrafine Aerosol Network (GUAN) [*Birmili et al.*, 2009]. GUAN provides continuous measurements of atmospheric aerosols in environments as diverse as street canyons, urban residential areas, regional background, and also mountain sites across Germany. As far as they are relevant to this study, information on the GUAN measurements are summarized in Table 1. Aerosol absorption is continuously measured by multiangle absorption photometers (MAAP; section 2.3). Parts of the filter samples collected by the MAAP were reanalyzed using Raman spectroscopy (section 2.2). In addition to these measurements, particle number size distributions are collected continuously by twin differential mobility particle sizers (TDMPS) or scanning mobility particle sizers (SMPS). For a number of selected days, size-segregated chemical particle composition is available from Berner impactor samples.

2.2. Raman Spectrometry

[9] To measure the Raman spectrum of atmospheric particles, a near-infrared Fourier transform (NIR-FT) spectrometer was coupled with a Raman-Module FRA-106 (Bruker Daltonik, Bremen, Germany). The monochromatic light source is a Nd:YAG Laser with a wavelength of 1064 nm. The sample is illuminated over a mirror arrangement so that incoming and Raman-scattered light do not interact. Directly reflected light and the Rayleigh-scattered light are removed by a filter module, because their intensities are much larger than the light from Raman scattering. An interferometer is used to measure the Raman-scattered light at different wavelengths. From there, the light is passed to a Ge-diode detector, which needs to be cooled with liquid nitrogen to achieve highest sensitivity. Fourier transformation is used to convert the Raman-scattered intensity from a function of the mirror shift to a function of wave number. This wave number is the so-called Raman shift. For the present study, the laser power was adjusted to 530 mW and the spectral resolution was set to 8 cm^{-1}. The filter samples were illuminated with a defocused beam in order to avoid a strong heating of the samples and to measure the average spectrum of a circular area with a diameter of approximately 1 mm. Wavelength calibration was always performed before the measurement using the characteristic band of a Nylon sample. All measurements were recorded as averages of 2900–3000 single spectra.

2.3. Multi Angle Absorption Photometer (MAAP)

[10] The MAAP is designed to continuously measure the aerosol absorption coefficient [*Petzold and Schönlinner*, 2004]. The GUAN network generally deploys MAAPs of the same type (model 5012, Thermo Scientific Inc.). Briefly, monochromatic light of a wavelength of 637 *nm* is transmitted and reflected from a particle-laden glass microfiber filter medium (GF10, Whatman, Maidstone, Kent). If particles are deposited on the glass microfiber filter, they only penetrate into the uppermost layer of the medium. Filter matrix and particles are subsequently treated as a two-layer system. To derive the absorption coefficient of the deposited particles, the instrument calculates the radiative transfer through this two-layer system [*Petzold and Schönlinner*, 2004]. The MAAP yields a BC mass concentration m_{BC}, which is converted from the absorption coefficient σ_{ap} under the assumption of a mass absorption cross section $\alpha_{BC} = 6.6\ m^2\ g^{-1}$.

[11] We configured the MAAP so that the filter spot is loaded until the transmission decreases to 50%. In any case, a filter change was obligatory at midnight, in order to have daily samples for subsequent analysis. The flow rates of the individual instruments were adjusted to match the nominal inlet flow rates at each observation sites and were 7 L min^{-1} at Leipzig-TROPOS, 15 L min^{-1} at Leipzig-Eisenbahnstraße, 8 L min^{-1} at Melpitz, 15 L min^{-1} at Bösel, 16 L min^{-1} at Hohenpeißenberg, 12 L min^{-1} at Schauinsland,

Table 1. Overview of the Measurement Sites and Instrumentation Used in This Work[a]

Observation Site	Type	Operator	Location	Altitude	Cont. Meas.	Discont. Meas.
Leipzig-Eisenbahnstrasse	traffic	Tropos-Leipzig	51.34° N, 12.37°	90 m	TDMPS[b] + TD[c], MAAP[d]	Raman[e], Berner[f]
Leipzig-TROPOS	urban	Tropos-Leipzig	51.34° N, 12.37° E	90 m	TDMPS[b] + TD[c], MAAP[d]	Raman[e], Berner[f]
Bösel	regional	GAA[h]	53.00° N, 7.97° E	13 m	SMPS[g] + TD[c], MAAP[d]	Raman[e], Berner[f]
Melpitz	regional	Tropos-Leipzig	51.54° N, 12.93° E,	86 m	TDMPS[b] + TD[c], MAAP[d]	Raman[e], Berner[f]
Hohen-peissenberg	mountain	DWD[i]	47.80° N, 11.00° E	988 m	SMPS[g] + TD[c], MAAP[d]	Raman[e], Berner[f]
Schauinsland	mountain	UBA[j]	47.91° N, 7.91° E	1210 m	SMPS[g] + TD[c], MAAP[d]	Raman[e], Berner[f]
Zugspitze	alpine mountain	UBA[j] and DWD[i]	47.42° N, 10.98° E	2650 m	SMPS[g] + TD[c], MAAP[d]	Raman[e]

[a]For more information on the GUAN network, see https://wiki.tropos.de.
[b]TDMPS (Twin Differential Mobility Particle Sizer), number size distribution between 3 and 800 nm.
[c]TD (Thermodenuder), evaporates volatile compounds at 300°C.
[d]MAAP (Multiangle Absorption Photometer), absorption coefficient at a wavelength of 637 nm.
[e]Raman (Raman spectrometer), mass concentration of C_{soot}.
[f]Berner (five-stage Berner impactor), particle sampling in five diameter classes between 0.05 and 10 μm for chemical analysis.
[g]SMPS (Scanning Mobility Particle Sizer), number size distribution between 10 and 800 nm.
[h]GAA (Trade supervisory office Hildesheim).
[i]DWD (German weather service).
[j]UBA (German Federal Environment Agency).

and 11 L min^{-1} at Zugspitze. The temporal resolution of the instruments was set to 1 min.

2.4. Thermographic Method

[12] The thermographic method is described in more detail in *Nordmann et al.* [2009] and will only be briefly summarized here. Particulate carbon on Berner impactor aluminium foils was characterized in compliance with guideline *VDI* [1999] using a carbon analyzer (Ströhlein, C-mat 5500). The organic carbon fraction (OC) was determined by heating an aliquot of the aluminium foils to 650 °C in a nitrogen atmosphere. The carbon that evaporates under these conditions is oxidized to CO_2 on a CuO catalyst at 850 °C and measured by using a NDIR detector. The elemental carbon fraction (EC) was determined by further heating the sample under oxygen atmosphere at 650 °C, oxidizing all carbon to CO_2, which was measured by the NDIR detector. Foil blank values were subtracted from the results. No charring correction could be applied, since the particles were sampled on aluminium foils. This may lead to an underestimation of OC and an overestimation of EC [*ten Brink et al.*, 2004]. Typical measurement uncertainties of 5.5% for OC and 8.9% for EC were determined for mass concentrations typical for atmospheric conditions [*Neusüss et al.*, 2000].

3. Calibration of the Raman Spectrometer

3.1. Raman Spectrum of Soot

[13] Freshly emitted soot particles are aggregates of spherules containing graphene layers, which are often rolled up to onion-like structures and might be mixed with other chemical compounds. The Raman spectrum of soot particles is usually composed of five overlapping bands [*Sadezky et al.*, 2005], originating from different excitations in the soot structure. An exemplary Raman spectrum of an atmospheric particle sample is shown in Figure 1. The G band around 1600 cm^{-1} can be attributed to vibrations in the graphitic lattice. In comparison with the G band of pure graphite (1580 cm^{-1}), the G band of Figure 1 appears shifted because of an overlapping band attributed to vibrations at the edge of graphite crystals. Such a shift of the G band was observed in previous Raman studies of atmospheric particle samples [*Dippel and Heintzenberg*, 1999; *Ivleva et al.*, 2007]. A second maximum, dominated by the D band, is located at around 1300 cm^{-1}. We often observed a shoulder on the lower energy side of the D band that can be attributed to stretching vibrations in polyene-like structures [*Dippel et al.*, 1999]. Signals characteristic for graphite can be clearly seen in the Raman spectra; the carbonaceous species detected by Raman spectroscopy is usually designated as graphitic carbon (GC). Details on the extraction of the G band integral from the Raman spectra are described in the supporting information.

3.2. Reference Material

[14] In order to calibrate the Raman spectrometer for C_{soot} determination, we tested the usability of furnace soot Printex®90 (Degussa AG, Essen, Germany) as a calibration material. Printex 90 particles were first deposited on GF10 filter samplers connected to a mixing chamber (as will be described in section 3.3) and then characterized by Raman spectroscopy. Raman spectra of Printex 90, atmospheric particles, and the blank filter show that the location of the G band agrees very well for the test particles and the atmospheric sample (Figure 1). A minor difference is that the D band position of Printex 90 is slightly shifted to lower wave numbers. The number size distribution of Printex 90 measured with a SMPS was monomodal, with a geometric mean diameter around 85 nm and a geometric standard deviation

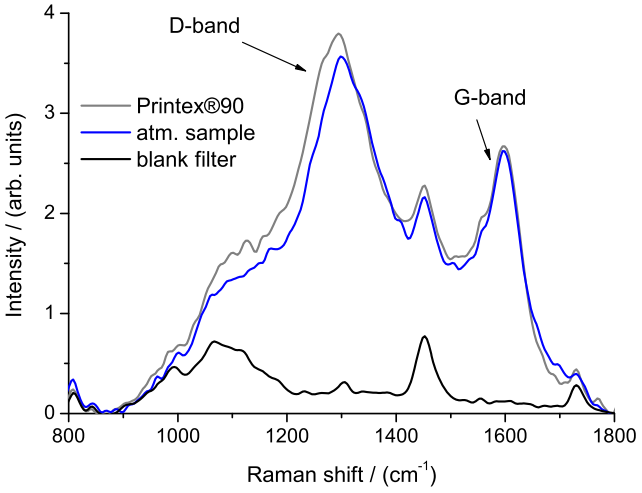

Figure 1. Comparison of Raman spectra of Printex®90, atmospheric particles, and the blank filter substrate. Major bands of the soot-containing samples are designated as G and D band.

of 1.9. (Atmospheric soot tends to be monomodal as well, with a similar mean diameter; see, e.g., *Rose et al.* [2006]). The primary Printex 90 particle size is around 14 nm; thus, we assume that particles aggregated in the mixing chamber.

[15] Since Raman spectroscopy is sensitive to GC, we require the calibration material to have a similar GC fraction as atmospheric particles. Therefore, the fractions of GC in Printex 90 and atmospheric samples were compared. A thermographic method, as described above, with an additional 850 °C temperature stage was first applied on pure graphite samples (Graphite Powder Natural, Alfa Aesar, and Graphite puriss., Sigma Aldrich). It was found that the graphite was only pyrolized in the last heating step. Applying the same procedure on Printex 90 particles and on atmospheric $PM_{2.5}$ samples deposited on quartz filters, the ratio between GC and the nonorganic total carbon (EC + GC) was derived. Table 2 shows that the GC fraction was very similar in Printex 90 and atmospheric soot particles. The contribution of carbonate carbon to nonorganic total carbon in atmospheric samples was considered negligible because concentrations at the sampling site Melpitz are generally low [*ten Brink et al.*, 2004].

[16] Graphitic structures in atmospheric soot particles are responsible for the broadband light absorption [*Bond and Bergstrom*, 2006]. The body of these results suggests that the basic structural properties of Printex 90, referring both to graphitic grid structure, particle size, and GC mass fraction, are similar enough to those of atmospheric soot particles to serve as a calibration standard for the Raman method. Following *Andreae and Gelencsér* [2006], Printex 90 aerosol can be best described by C_{soot}, because the OC fraction is negligible and graphitic structures are obvious. In addition, transmission electron microscope pictures show the aggregate structure of small spherules [*Monteiro-Riviere and Inman*, 2006].

3.3. Experimental Setup

[17] The objective of the calibration experiment was to establish a relationship between the integral of the Raman G band and the gravimetric mass of Printex 90. In the experiment, a hydrosol of distilled water and Printex 90 was nebulized. This aerosol passed through a silica gel drier and a bipolar diffusion charger before entering into the mixing chamber. The concentration was controlled by adjusting the pressure drop across the nebulizer and roughly checked with the MAAP. Polycarbonate filters with a pore size of 100 nm (Nuclepore™, Whatman, Maidstone, Kent), glass microfiber filters (GF10, Whatman, Maidstone, Kent), and quartz fiber filters (Pallflex®, Pall, New York, USA) were loaded simultaneously, with constant flow rates assured by mass flow controllers. The glass microfiber filter corresponds to the medium used inside the MAAP and is used for Raman spectroscopy after sampling. A microbalance (UMT, Mettler Toledo) was used to weigh the polycarbonate and quartz fiber filters. The flow ratio between the different filter samplers was used to reconstruct the gravimetric mass loading of the microfiber filters, which were analyzed by Raman spectroscopy.

3.4. Calibration Results

[18] The results of the calibration experiment can be seen in Figure 2, suggesting a linear relationship between the mass loading of Printex 90 and the corresponding G band integral. The range covered by the experiment is typical for the mass loadings encountered in the MAAP, i.e., with minimum transmission set to 50%. An error-weighted orthogonal regression yields a slope of 0.00681 and an offset of 0.332. The measure of determination (R^2) was 0.95. When applying these calibration results on atmospheric particle samples, a C_{soot} Printex 90 equivalent is determined. We established a calibration function to derive the C_{soot} mass concentration as follows:

$$m_{C,\mathrm{soot}} = \frac{m \cdot A}{\Delta t \cdot q}, \tag{1}$$

with m being the particulate mass on the filter using the results of the orthogonal regression, Δt the sampling duration, A the loaded filter area, and q the volumetric flow rate.

[19] The uncertainties of the integral over the G band were estimated by repeating the Raman measurements for selected filters. On average, an uncertainty of 7.5% was found. The error of m was estimated by Gaussian error propagation using the uncertainties of the spot diameter (5%), the flow ratio (7%) and the Printex 90 mass on the weighed filter samples (6%). On average, an error of 15% was found for m on the glass microfiber filter. The uncertainty of the fit function was derived as a byproduct of the orthogonal regression procedure to be 1.4% for the slope and 4% in offset.

Table 2. Average and Standard Deviation of the GC Fraction in the Nonorganic Total Carbon for Atmospheric, Graphite, and Printex®90 Samples

Sample	n	μ	σ
Printex 90	4	0.20	0.06
atmospheric sample[a]	9	0.21	0.08
graphite[b]	4	0.99	0.02

[a]Collected at the rural background site Melpitz.
[b]Aggregate of two samples of synthetic and natural graphite, respectively.

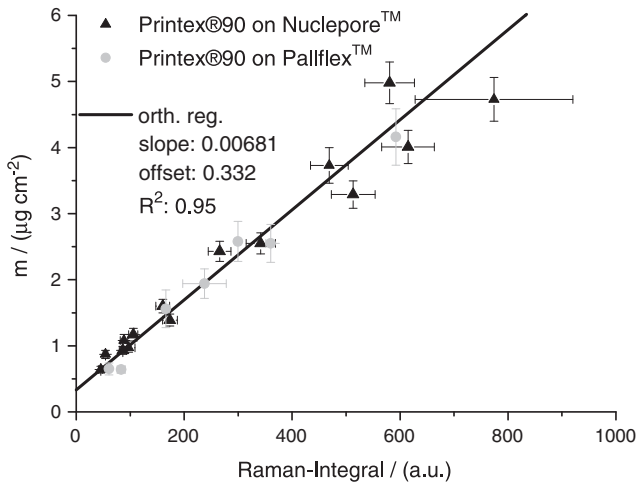

Figure 2. Relation between gravimetric mass of Printex®90 and corresponding integral over the G band in the Raman-Spectrum. Black dots indicate the usage of a polycarbonate filter and red dots of a quartz filter.

4. Field Observations

4.1. Selection of Measurement Periods

[20] Processing particle samples with Raman spectroscopy requires considerable time. Therefore, we focused on the analysis of field samples from three selected episodes within the years 2009 and 2010. In Central Europe, major differences arise between different air masses from the climatologically relevant contrast between maritime and continental air [*Birmili et al.*, 2001]. To classify periods of pronounced maritime ("m") or more continental ("c") air masses, 72 h backward trajectories were calculated using the HYSPLIT model [*Draxler and Hess*, 1997].

[21] Three selected episodes covered the periods between 25 March and 10 April 2009 (Episode I), between 29 May and 20 June 2009 (Episode II), and between 24 and 31 January 2010 (Episode III). Episode I was characterized by a transition from a maritime to a continental air mass in early summer. Episode II represented a continuous period of maritime air masses over Central Europe. Episode III was characterized by a continental air mass in winter, with a high pressure area residing over Central Europe and the presence of a pronounced temperature inversion. In a later stage, this continental air mass was replaced by a very clean air mass of Arctic origin.

[22] For a detailed discussion, the Episodes I and III are split into different parts: Im and Ic, and IIIc and IIIm to distinguish between the maritime and continental air mass types. Episode II is denoted IIm to emphasize the maritime character of that air mass. Figure 3 shows illustrative back trajectories for each of these periods.

4.2. Observations of $m_{C,soot}$ and σ_{ap}

[23] Figure 4 compiles the C_{soot} mass concentrations $m_{C,soot}$, absorption coefficients σ_{ap} and mass absorption cross sections $\alpha_{C,soot}$ for all periods where Raman measurements were performed.

[24] The maritime Episode Im featured $m_{C,soot}$ between 0.1 $\mu g\,m^{-3}$ at the mountain location Zugspitze and 4 $\mu g\,m^{-3}$ at the kerbside observation site Leipzig-Eisenbahnstrasse. The absorption coefficients σ_{ap} obtained from the MAAP showed a corresponding span between 0.2 and 18 Mm^{-1}. After the continental air mass arrived over Central Europe on 1 April 2009, $m_{C,soot}$ increased to values between 0.5 and 15 $\mu g\,m^{-3}$ with corresponding values of σ_{ap} between 2 and 55 Mm^{-1}. Details of the time series show that both signals are closely correlated. In Episode IIm, $m_{C,soot}$ ranged between 0.1 $\mu g\,m^{-3}$ at Zugspitze and 2.9 $\mu g\,m^{-3}$ at the urban background site Leipzig-TROPOS, respectively. The values of σ_{ap} ranged between 0.4 and 9.4 Mm^{-1}, accordingly. During Episode IIIc, $m_{C,soot}$ ranged between 0.2 $\mu g\,m^{-3}$ at Zugspitze and 20 $\mu g\,m^{-3}$ at Leipzig-TROPOS, with corresponding σ_{ap} residing between 1.2 and 104 Mm^{-1}. After the replacement of the air mass by maritime air on 27 January 2010, a rapid drop can be seen in all experimental values. Episode IIIm exhibited $m_{C,soot}$ values between merely 0.07 and 2.4 $\mu g\,m^{-3}$, and σ_{ap} between 0.4 and 10 Mm^{-1}. To sum up, the five selected episodes represent a wide variety of Central European air mass observations, which is reflected in the wide range of observed $m_{C,soot}$ and σ_{ap}. It can also be seen that the absolute concentrations varied strongly as a function of location, with high values near source (kerbside, urban background) and little values at elevated mountain sites.

4.3. Calculations of $\alpha_{C,soot}$

[25] The mass absorption cross section $\alpha_{C,soot}$ is visualized as gray lines in Figure 4. The corresponding correlations were analyzed for each sub-episode using orthogonal regression (see Figure 5). The regression coefficients for individual measurement sites are compiled in Table 3. The axis offsets of the fit curves were insignificantly different from zero, and the correlations tended to have good measures of determination, often better than 0.90.

[26] It is an essential result of this paper that the observed differences in $\alpha_{C,soot}$ between the measurement sites and air masses were relatively minor. Despite having been taken

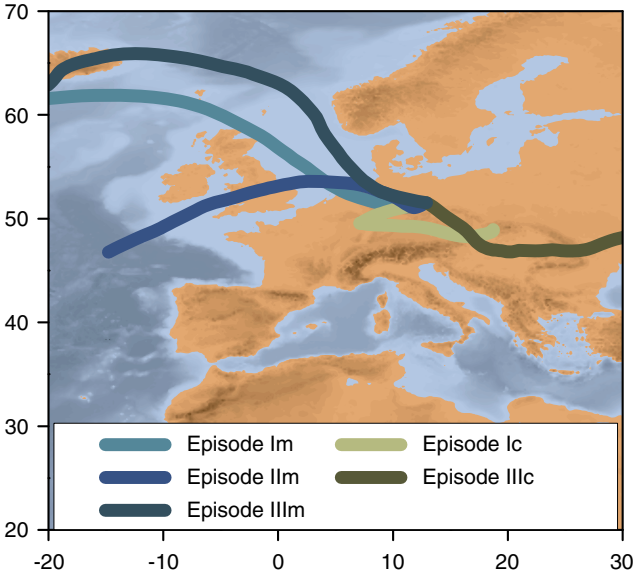

Figure 3. Selected 72 h back trajectories illustrating the origin of the air masses Im, Ic, IIm, IIIc, and IIIm discussed in the text.

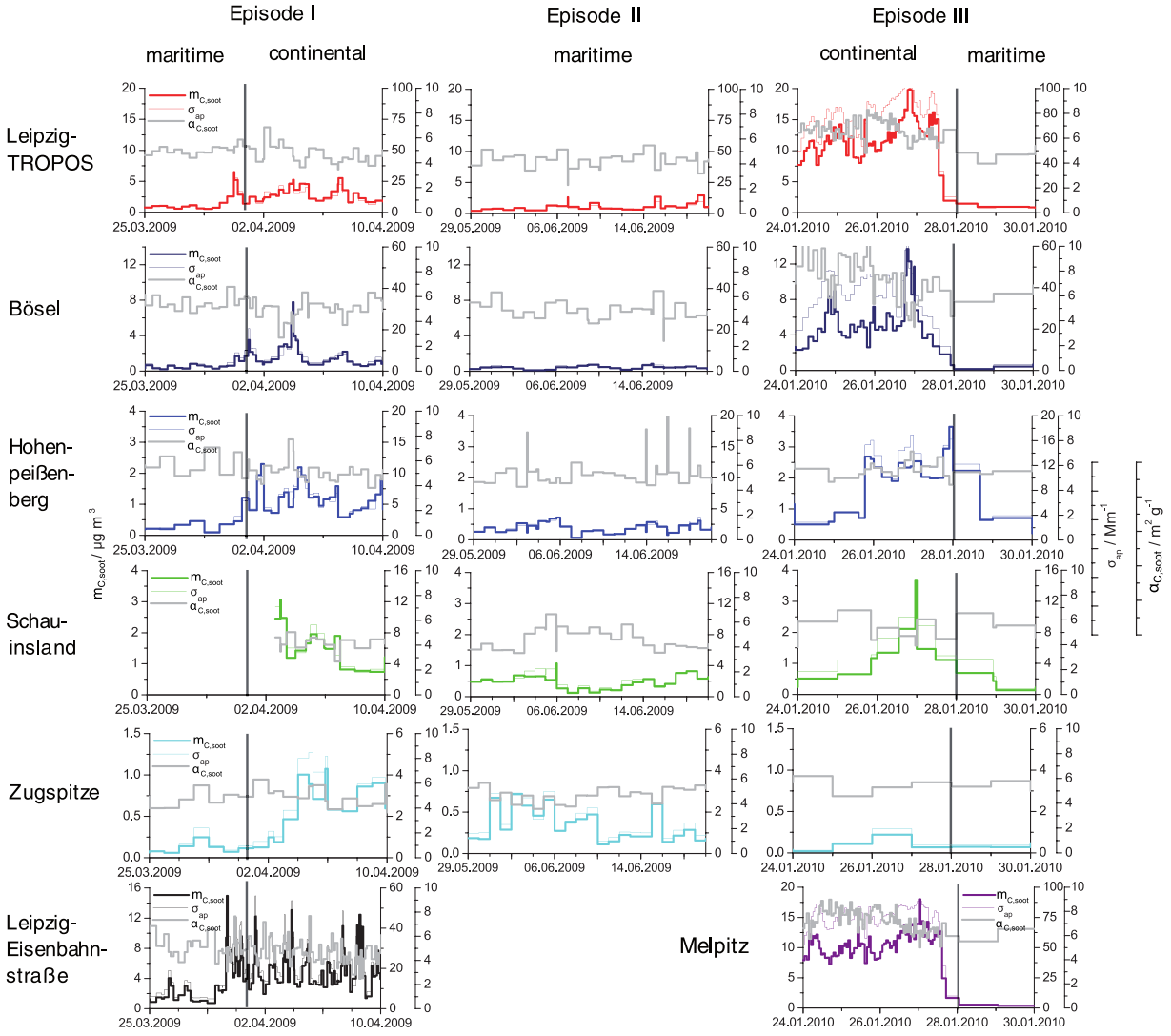

Figure 4. Overview of in situ measurements during Episodes I, II, and III: Time series of the C_{soot} mass concentration $m_{C,soot}$, absorption coefficient σ_{ap} and mass absorption cross section $\alpha_{C,soot}$ at seven observation sites of the German Ultrafine Aerosol Network (GUAN). In episodes I and III, the change from maritime to continental air and vice versa is indicated by a vertical line.

under diverse circumstances, the variation in $\alpha_{C,soot}$ across the body of samples is only about 17% around an overall value of 5.3 m^2 g^{-1}, determined by orthogonal regression. For Episode I, the range of values was 4.2–5.8 m^2 g^{-1}, for Episode II, 4.2–5.1 m^2 g^{-1} (Table 3). Note that this span includes observations at all measurement sites. Only during Episode III, an enhanced span of $\alpha_{C,soot}$ was observed, ranging between 3.9 and 7.4 m^2 g^{-1}.

[27] The lowest value with 4.1 m^2 g^{-1} was observed during the clean maritime summer air mass in Episode IIm. The maximum value of 6.4 m^2 g^{-1} was determined for the continental winter Episode IIIc (see Figure 5).

5. Discussion

5.1. Variability of the Mass Absorption Cross Section

[28] Although this work observed only minor variations in the mass absorption cross section $\alpha_{C,soot}$ around a mean value of 5.3 m^2 g^{-1}, a remarkable feature was the enhanced value of 6.4 m^2 g^{-1} in a highly concentrated pollution aerosol in the winter Episode III. We will discuss here the possible reasons for the observed variabilities in $\alpha_{C,soot}$.

[29] The variations may first derive from contributions of non-soot particles to light absorption. Organic aerosol particles have been acknowledged to contribute to the light absorption coefficient [*Andreae and Gelencsér*, 2006], although the absorption spectrum steeply declines to the wavelength measured by the MAAP instrument [*Sun et al.*, 2007]. *Favez et al.* [2009] suggested, for example, that the contribution of the organic fraction of a biomass burning aerosol to absorption amounts to no more than 8%. The effect of biomass burning (e.g., wood) aerosol on the Raman spectrum is not well-known. In a previous study, we compared the Raman spectra of atmospheric and freshly emitted wood-burning particles deposited on Pallflex filters. Therefore, the soot signal in the Raman spectrum was fitted using four bands. We added the statistic for the two major

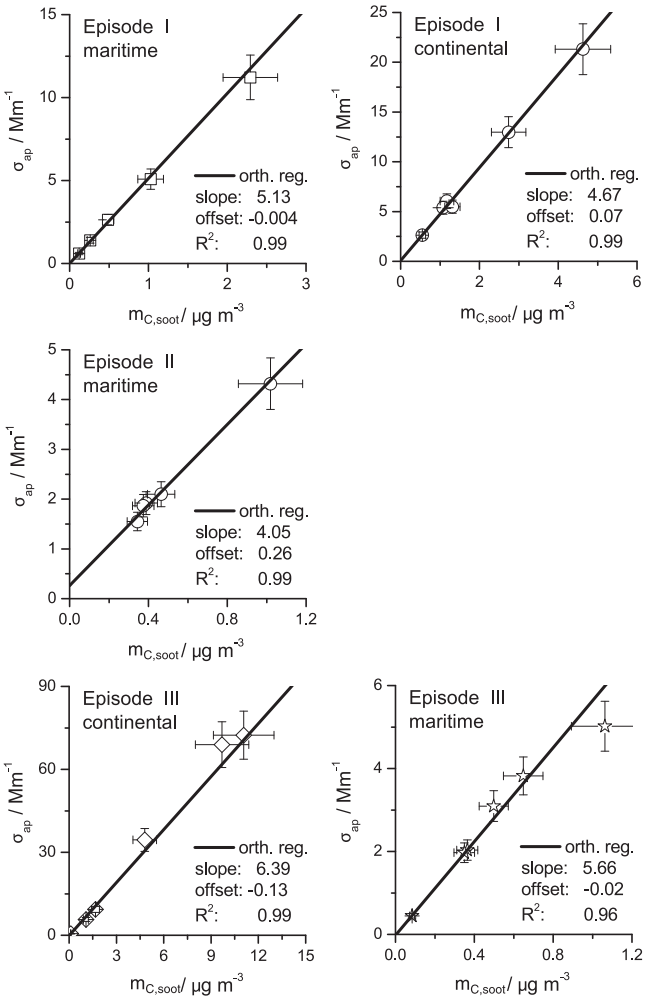

Figure 5. Scatterplot between the mass concentration of C_{soot} ($m_{C,soot}$) and the absorption coefficient (σ_{ap}) for air masses prevailing during Episode I, Episode II, and Episode III. Each data point represents the average values at individual measurement sites. Slopes and offsets are determined considering the errors in both variables and by orthogonal regression.

bands (G and D, as described in section 3.1) to the supporting information. It can be seen that the full width at half maximum (FWHM) for the D and the G bands is higher for wood-burning particles than for atmospheric particles. Simultaneously, the intensity ratio between the D and G band differs only insignificantly. Adopting this to the present study, one could expect an increased FWHM of the G band if a large fraction of particles originate from wood-burning sources. This would lead to an increase of the integral of the G band and therefore an overestimation of C_{soot}. If the absorption coefficient is not influenced by such particles, a lower mass absorption cross section would be expected. This excludes biomass-burning aerosol as a potential reason for the enhanced mass absorption cross section during Episode III.

[30] An additional absorber of radiation is mineral dust. Since its absorption is correlated with the particle number concentration greater than 1 µm [*Müller et al.*, 2009a] at least in the near-field of sources, a negligible influence is expected only on PM_1 absorption even if significant amounts of dust were present. In addition, the absorption coefficients of mineral dust decrease strongly with increasing wavelength [*Petzold et al.*, 2009]. For this reason, no effect of mineral dust on the mass absorption cross section is expected from the present study.

[31] Our hypothesis is that the observed variability in $\alpha_{C,soot}$ is due to changes in the state of mixture. Theoretical studies based on Mie theory predict that the mass absorption cross section increases as particles get mixed with non-absorbing material [*Fuller et al.*, 1999]. Several studies have analyzed laboratory-generated as well as ambient soot particles with regard to the effect of a coating on their mass absorption cross section [e.g., *Khalizov et al.*, 2009; *Naoe et al.*, 2009; *Shiraiwa et al.*, 2010]. All these authors found that the mass absorption cross section increases if particles are coated with non-absorbing material. The changes reported in the mass absorption cross section from laboratory and field measurement are between 25 and 50% as the shell volume fraction is between 50 and 88% [*Shiraiwa et al.*, 2010; *Naoe et al.*, 2009].

[32] The enhanced value of 6.4 $m^2\ g^{-1}$ in this work was measured in a highly concentrated pollution aerosol, which featured PM_{10} mass concentrations over several days up to 250 µg m^{-3} (Episode IIIc). Although we have no experimental evidence, it is plausible to assume that in such a concentrated aerosol, coagulation among particles played a certain role, and was thus instrumental in changing the mixing state of soot. However, other processes like coating of soot by the condensation of, e.g., organics seem possible as well [*Shiraiwa et al.*, 2007].

5.2. Comparison With Elemental Carbon (EC)

[33] It is helpful to compare the mass concentrations of C_{soot} with standardized measurements of elemental carbon (EC) from the thermographic method described in section 2. (EC was available for certain days at 24 h time resolution.) Figure 6 shows a reasonable quantitative agreement (R^2 = 0.87, slope = 1) for the regional background samples. Like for C_{soot}, mass absorption cross sections were determined for EC (α_{EC}) by orthogonal regression between mass concentrations of EC from Berner impactor samples and σ_{ap}. It is important to note that the Berner impactor samples were collected across the entire years 2009 and 2010 and cover a large spectrum of synoptic situations. The results for the GUAN measurement sites are summarized in Table 3. Values of α_{EC} ranged between 4.3 and 6.8 $m^2\ g^{-1}$ and therefore matched the range of values of $\alpha_{C,soot}$ very well.

[34] Uncertainties of the thermographic method are due to the missing charring correction, which may lead to an overestimation of EC. Simultaneously, a GC fraction might be missing because Berner samples could only be heated up to 650°C. On the other hand, C_{soot} from Raman includes both EC and GC. So the good agreement between EC and C_{soot} might be due to a compensation of the missing GC fraction by charring contribution to EC during thermographic analysis.

5.3. Comparison With Literature Results

[35] In Table 4, a compilation of different studies determining soot mass absorption cross sections is shown. In these studies, the variation in the mass absorption cross

Table 3. Results of Orthogonal Regressions With Slope (Characteristic Value of $\alpha_{C,soot}$ in $m^2\ g^{-1}$) and Coefficient of Determination (R^2) Between the Mass Concentration of C_{soot} ($m_{C,soot}$) and the Absorption Coefficient (σ_{ap})[a]

	Episode I				Episode II		Episode III				Berner	
	m		c		m		c		m			
	Slope	R^2	Slope	R^2	Slope	R^2	Slope	R^2	Slope	R^2	Slope	R^2
Leipzig-Eisenbahnstrasse	4.60	0.86	4.62	0.75	-	-	-	-	-		6.75	0.65
Leipzig-TROPOS	5.07	0.99	5.11	0.86	4.21	0.73	6.58	0.68	4.23	0.96	6.34	0.77
Bösel	5.50	0.90	5.21	0.93	5.00	0.84	6.42	0.53	5.99	0.97	4.57	0.84
Melpitz	-	-	-	-	-	-	7.39	0.63	5.45	0.98	4.43	0.84
Hohen-peissenberg	4.43	0.97	4.58	0.85	5.11	0.77	6.11	0.86	5.24	0.99	4.32	0.75
Schauinsland	-	-	4.21	0.87	4.29	0.81	4.29	0.94	5.82	0.97	6.41	0.48
Zugspitze	5.81	0.98	4.79	0.81	3.97	0.96	4.91	0.99	3.85	0.98	-	-

[a]The data of the three episodes were divided into different air masses (m = maritime, c = continental) and Berner samples of 2009 and 2010 were analyzed.

section has often been attributed by authors to changes in the state of mixture of soot particles. However, the values in Table 4 show a large span between 3.6 and 18.3 $m^2\ g^{-1}$, which is probably also due to different measurement devices. Overall, the values measured in our study are at the lower bound of the cited mass absorption cross sections.

[36] For a more confident comparison with our values, only studies using the MAAP were considered. In this case, an average mass absorption cross section of $6.7\pm2.2\ m^2\ g^{-1}$ is derived, which is in good agreement with the value suggested by *Bond and Bergstrom* [2006]. This span is narrower and also closer to $\alpha_{C,soot}$ from our study. Besides the MAAP, another widely used absorption measurement device is the particle soot absorption photometer (PSAP), which measures only the transmission of light (550 nm) through a particle laden filter medium. Averaging the mass absorption cross sections based on PSAP measurements, a value of $12.8\pm2.3\ m^2\ g^{-1}$ is derived. Converting the MAAP value to the PSAP wavelength of 550 nm using an Angström exponent of –1, a value of $7.8\ m^2\ g^{-1}$ can be derived. This 40% difference between PSAP and MAAP mass absorption cross sections cannot be explained by a wrong assumption of the Angström exponent. Four studies using the photoacoustic method for measuring the absorption coefficient are listed in Table 4. Adjusting these studies to the PSAP and MAAP wavelengths with an Angström exponent of –1, an average mass absorption cross section of $9.2\pm4.1\ m^2\ g^{-1}$ and $7.9\pm3.5\ m^2\ g^{-1}$ is calculated, respectively. This is higher than values from the present study, but lower by around 30% in comparison to mass absorption cross sections from PSAP measurements. It is well-known that PSAP absorption coefficients have to be corrected for spot size, flow rate, filter loading, and the presence of scattering particles. In principle, this is done by the correction method presented in *Bond et al.* [1999]. Another method is published by *Virkkula et al.* [2005] and gives absorption coefficients that are approximately 6% higher for single scattering albedos between 0.8 and 0.9 [*Müller et al.*, 2011]. In presence of strongly scattering material like mineral dust in the samples, an additional correction should be applied [*Müller et al.*, 2009b]. If the mass absorption cross sections from PSAP measurements are used, one has to assure which correction was applied on the data and, if necessary, a more appropriate method should be used.

[37] Besides potential uncertainties in absorption coefficient measurements, also EC concentrations from different thermal methods may vary by a factor of 3 [*ten Brink et al.*, 2004], which may contribute to the large variation of mass absorption cross sections summarized in Table 4. However, in comparison to previous literature values, the mass absorption cross section in the present study shows a much smaller variability, although the samples were taken in quite diverse environments. It has to be noted, that the inter-instrumental variability was very small because of the usage of only one Raman spectrometer in combination with several MAAPs (variability <5%, *Müller et al.* [2011]).

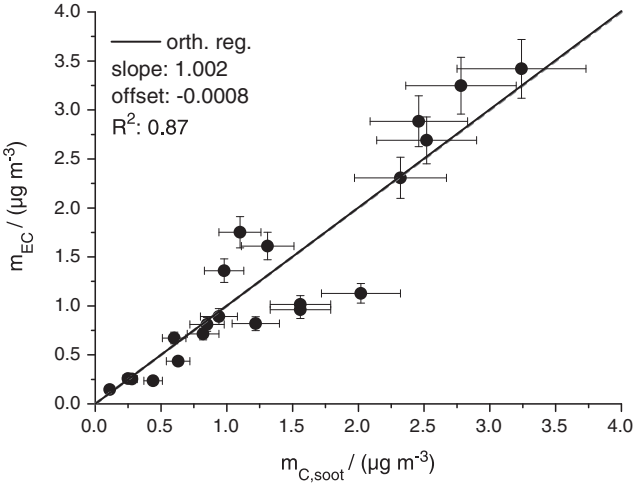

Figure 6. Comparison between daily averaged mass concentrations of C_{soot} ($m_{C,soot}$) from Raman spectroscopy and corresponding mass concentrations of elemental carbon (m_{EC}) from thermographic analysis of daily Berner impactor samples.

Table 4. Compilation of Previous Experimental Studies of the Soot Mass Absorption Cross Section

Site	Type	Author	Absorption Measurement	Carbon Measurement	Mass Absorption Cross Sections (m^2 g^{-1})
Jungfraujoch, Switzerland	mountain	*Cozic et al.* [2008]	MAAP (637 nm)	EC/OC[a]	7.4–11.1
Manora Peak, India	mountain	*Ram et al.* [2010]	optical attenuation (687 nm)	EC/OC[a]	11.6–14.5
Maledives (aircraft)		*Mayol-Bracero et al.* [2002]	PSAP (550 nm)	EC/OC[b]	8.1
Manaus, Brazil	regional	*Gilardoni et al.* [2011]	MAAP (637 nm)	EC/OC[c]	4.7
Guangzhou, China	regional	*Kondo et al.* [2009]	PSAP, COSMOS (565)[g]	EC/OC[a]	9.9–12.0
Yufa, China	regional	*Kondo et al.* [2009]	PSAP, COSMOS (565 nm)[g]	EC/OC[a]	11.6–15.7
Mexico City, Mexico	regional	*Doran et al.* [2007]	Photoacoustic (870 nm)	EC/OC[a]	8.5
Brighton, Colorado	regional	*Moosmüller et al.* [1998]	Photoacoustic (685 nm) (685 nm)	EC/OC[d]	3.6
Gosan, South Korea	regional	*Chuang et al.* [2003]	PSAP (550 nm)	EC/OC[a]	12.6–14.8
Finokalia, Greece	regional	*Sciare et al.* [2003]	PSAP	EC/OC[a]	7.5
kleiner Feldberg, Germany	regional	*Petzold and Schönlinner* [2004]	MAAP (637 nm)	EC/OC[e]	4.8
Tsukuba, Japan	regional	*Naoe et al.* [2009]	PSAP (565 nm)	EC/OC[d]	10–13
Berlin, Germany	urban	*Petzold and Schönlinner* [2004]	MAAP (637 nm)	EC/OC[e]	6.3
Vienna, Austria	urban	*Hitzenberger et al.* [2006]	MAAP (637 nm)	EC/OC[e]	3.9–8.4
Atlanta, USA	urban	*Carrico et al.* [2003]	PSAP (550 nm)	EC/OC[a e f]	5.3–18.3
Toronto, Canada	urban	*Knox et al.* [2009]	Photoacoustic (760 nm) (760 nm)	EC/OC[a]	6.9–9.9
Tokyo, Japan	urban	*Kondo et al.* [2009]	PSAP, COSMOS (565 nm)[g]	EC/OC[a]	6.7–15.0
Laboratory	coated flame soot	*Khalizov et al.* [2009]	extinction-scattering (532 nm)[h]	DMA/ APM	8.7–12.6
Laboratory	coated graphite	*Shiraiwa et al.* [2010]	Photoacoustic (532 nm)	SP2[i]	5.1 – 10

[a]EC/OC analyzer Sunset Laboratory, as described in *Birch and Cary* [1996].
[b]EC/OC by Evolved Gas Analysis, EGA [*Novakov et al.*, 1997].
[c]EC/OC dual optical carbonaceous analyzer (Sunset Laboratory), EUSAAR2-protocol [*Cavalli et al.*, 2010].
[d]EC/OC by thermal/optical reflectance from Desert Research Institute (DRI) [*Chow et al.*, 1993].
[e]EC/OC by a thermal method following *VDI* [1996].
[f]EC/OC by a Rupprecht and Patashnick Series 5440 ambient carbon particulate monitor.
[g]σ_{ap} at 565 nm by a Continuous Soot Monitoring System (COSMOS, Kanomax, Osaka, Japan) *Miyazaki et al.* [2008].
[h]σ_{ap} at 532 nm by nephelometer and cavity ring-down spectrometer.
[i]BC by laser-induced incandescence as described in *Gao et al.* [2007].

6. Summary and Conclusions

[38] A new method for the determination of soot mass concentrations applying Raman-spectroscopy on particle samples collected on a filter medium commonly used in conjunction with multiangle absorption photometer (MAAP) measurements was developed. In a laboratory calibration, a linear relationship between gravimetric determined masses of test soot Printex®90 and the corresponding integral over the G band in the Raman-spectrum was found. The method was applied on particle samples from MAAP field measurements in the German Ultrafine Aerosol Network (GUAN). This combination of MAAP and Raman spectrometer enabled a determination of quantitative values of the mass absorption cross section of atmospheric C_{soot}. Since the data were collected at multiple observation sites from mountain to near traffic locations, the mass absorption cross sections can be regarded as representative for the continental boundary layer air over Central Europe.

[39] Particle samples of seven observation sites taken in two summer and one winter time period were analyzed. The results showed that the variation of the mass absorption cross sections between individual measurement sites and for different air masses was only small, especially during the summer episodes. For the winter episode, the mass absorption cross section was slightly higher. Average values varied between 3.9 and 7.4 m^2 g^{-1}, depending on measurement site and observational period. Overall, a value of 5.3 m^2 g^{-1} is deemed suitable for C_{soot} in the Central European troposphere.

[40] The connection of the new Raman method to a commonly used thermographic method for EC was established by the fact that the mass concentrations of EC and C_{soot} were in good agreement, at least for the regional observation site Bösel. Furthermore, the mass absorption cross section of EC was in good agreement with that for C_{soot}. The mass absorption cross section of C_{soot} was found to be lower in comparison to values from previous studies (mostly for EC).

The largest deviations were found for studies in which the particle soot absorption photometer (PSAP) was applied.

[41] The mass absorption cross section of soot particles is a vital parameter for projections of climate forcing. The findings of the present study could imply that current estimates of aerosol radiative forcing (for Central Europe), such as determined from radiative transfer models, might be positively biased. Moreover, many instrumental methods (such as the Aethalometer, PSAP, or MAAP) rely on the use of a mass absorption cross section to convert light absorption into a soot mass concentration. The present results suggest that the currently used conversion factors might be too high for this purpose.

[42] **Acknowledgments.** This work was supported by the German Federal Ministry for the Environment, Nature Conservation and Nuclear Safety (BMU) grants F&E 370343200 (German title: *"Erfassung der Zahl feiner und ultrafeiner Partikel in der Aussenluft"*) and F&E 371143232 (German title: *"Trendanalysen gesundheitsgefährdender Fein- und Ultrafeinstaubfraktionen unter Nutzung der im German Ultrafine Aerosol Network (GUAN) ermittelten Immissionsdaten durch Fortführung und Interpretation der Messreihen"*). Stephan Nordmann acknowledges support by a personal scholarship of the Deutsche Bundesstiftung Umwelt (DBU). We are grateful to Harald Flentje (DWD Hohenpeissenberg), Ludwig Ries (UBA Zugspitze), and Frank Meinhardt (UBA Schauinsland) for assistance with the collection of MAAP data and Berner impactor samples. We furthermore acknowledge Thomas Gnauk (TROPOS Leipzig) for EC/OC analyses of graphite samples and André Sonntag for TDMPS and SMPS data processing.

References

Ackerman, A., O. Toon, D. Stevens, A. Heymsfield, V. Ramanathan, and E. Welton (2000), Reduction of tropical cloudiness by soot, *Science*, *288*(5468), 1042–1047, doi:10.1126/science.288.5468.1042.

Andreae, M., and A. Gelencsér (2006), Black carbon or brown carbon? The nature of light-absorbing carbonaceous aerosols, *Atmos. Chem. Phys.*, *6*(10), 3131–3148, doi:10.5194/acp-6-3131-2006.

Baumgardner, D., et al. (2012), Soot reference materials for instrument calibration and intercomparisons: A workshop summary with recommendations, *Atmos. Meas. Tech.*, *5*(8), 1869–1887, doi:10.5194/amt-5-1869-2012.

Birch, M., and R. Cary (1996), Elemental carbon-based method for monitoring occupational exposures to particulate diesel exhaust, *Aerosol Sci. Technol.*, *25*(3), 221–241, doi:10.1080/02786829608965393.

Birmili, W., A. Wiedensohler, J. Heintzenberg, and K. Lehmann (2001), Atmospheric particle number size distribution in Central Europe: Statistical relations to air masses and meteorology, *J. Geophys. Res.*, *106*(D23), 32,005–32,018.

Birmili, W., et al. (2009), Atmospheric aerosol measurements in the German Ultrafine Aerosol Network (GUAN): Part 1. Soot and particle number size distributions, *Gefahrst. Reinh. Luft*, *69*(4), 137–145.

Bond, T., and R. Bergstrom (2006), Light absorption by carbonaceous particles: An investigative review, *Aerosol Sci. Technol.*, *40*(1), 27–67, doi:10.1080/02786820500421521.

Bond, T., T. Anderson, and D. Campbell (1999), Calibration and intercomparison of filter-based measurements of visible light absorption by aerosols, *Aerosol Sci. Technol.*, *30*(6), 582–600, doi:10.1080/027868299304435.

Bond, T. C., D. G. Streets, K. F. Yarber, S. M. Nelson, J.-H. Woo, and Z. Klimont (2004), A technology-based global inventory of black and organic carbon emissions from combustion, *J. Geophys. Res.*, *109*, D14203, doi:10.1029/2003JD003697.

Carrico, C. M., M. H. Bergin, J. Xu, K. Baumann, and H. Maring (2003), Urban aerosol radiative properties: Measurements during the 1999 Atlanta Supersite Experiment, *J. Geophys. Res.*, *108*(D7), 8422, doi:10.1029/2001JD001222.

Cavalli, F., M. Viana, K. Yttri, J. Genberg, and J. Putaud (2010), Toward a standardised thermal-optical protocol for measuring atmospheric organic and elemental carbon: The EUSAAR protocol, *Atmos. Meas. Tech.*, *3*, 79–89, doi:10.5194/amt-3-79-2010.

Chow, J., J. Watson, L. Pritchett, W. Pierson, C. Frazier, and R. Purcell (1993), The DRI thermal/optical reflectance carbon analysis system: Description, evaluation and applications in US air quality studies, *Atmos. Environ.*, *27*(8), 1185–1201, doi:10.1016/0960-1686(93)90245-T.

Chuang, P. Y., R. M. Duvall, M. S. Bae, A. Jefferson, J. J. Schauer, H. Yang, J. Z. Yu, and J. Kim (2003), Observations of elemental carbon and absorption during ACE-Asia and implications for aerosol radiative properties and climate forcing, *J. Geophys. Res.*, *108*(D23), 8634, doi:10.1029/2002JD003254.

Cozic, J., et al. (2008), Chemical composition of free tropospheric aerosol for PM1 and coarse mode at the high alpine site Jungfraujoch, *Atmos. Chem. Phys.*, *8*(2), 407–423, doi:10.5194/acp-8-407-2008.

Dippel, B., and J. Heintzenberg (1999), Soot characterization in atmospheric particles from different sources by NIR FT Raman spectroscopy, *J. Aerosol Sci.*, *30*, suppl. 1, S907–S908, doi:10.1016/S0021-8502(99)80464-9.

Dippel, B., H. Jander, and J. Heintzenberg (1999), NIR FT Raman spectroscopic study of flame soot, *Phys. Chem. Chem. Phys.*, *1*(20), 4707–4712, doi:10.1039/A904529E.

Doran, J., et al. (2007), The T1-T2 study: Evolution of aerosol properties downwind of Mexico City, *Atmos. Chem. Phys.*, *7*(6), 1585–1598, doi:10.5194/acp-7-1585-2007.

Draxler, R., and G. Hess (1997), Description of the HYSPLIT4 modeling system, *NOAA Tech. Memo.*, NOAA Air Rescources Laboratory, Silver Spring, Md.

Favez, O., S. Alfaro, J. Sciare, H. Cachier, and M. Abdelwahab (2009), Ambient measurements of light-absorption by agricultural waste burning organic aerosols, *J. Aerosol Sci.*, *40*(7), 613–620, doi:10.1016/j.jaerosci.2009.04.002.

Forster, P., et al. (2007), Changes in atmospheric constituents and in radiative forcing, in *Climate Change 2007: The Physical Science Basis. Contribution of Working Group I to the Fourth Assessment Report of the Intergovernmental Panel on Climate Change*, edited by S. Solomon et al., pp. 129–234, Cambridge Univ. Press, Cambridge, U. K.

Fuller, K. A., W. C. Malm, and S. M. Kreidenweis (1999), Effects of mixing on extinction by carbonaceous particles, *J. Geophys. Res.*, *104*(D13), 15,941–15,954, doi:10.1029/1998JD100069.

Gao, R. S., et al. (2007), A novel method for estimating light-scattering properties of soot aerosols using a modified single-particle soot photometer, *Aerosol Sci. Technol.*, *41*(2), 125–135, doi:10.1080/02786820601118398.

Gilardoni, S., E. Vignati, E. Marmer, F. Cavalli, C. Belis, V. Gianelle, A. Loureiro, and P. Artaxo (2011), Sources of carbonaceous aerosol in the Amazon basin, *Atmos. Chem. Phys.*, *11*(6), 2747–2764, doi:10.5194/acp-11-2747-2011.

Heintzenberg, J. (1982), Size-segregated measurements of particulate elemental carbon and aerosol light absorption at remote Arctic locations, *Atmos. Environ.*, *16*(10), 2461–2469, doi:10.1016/0004-6981(82)90136-6.

Hitzenberger, R., A. Petzold, H. Bauer, P. Ctyroky, P. Pouresmaeil, L. Laskus, and H. Puxbaum (2006), Intercomparison of thermal and optical measurement methods for elemental carbon and black carbon at an urban location, *Environ. Sci. Technol.*, *40*(20), 6377–6383, doi:10.1021/es051228v.

Ivleva, N., U. McKeon, R. Niessner, and U. Pöschl (2007), Raman microspectroscopic analysis of size-resolved atmospheric aerosol particle samples collected with an ELPI: Soot, humic-like substances, and inorganic compounds, *Aerosol Sci. Technol.*, *41*(7), 655–671, doi:10.1080/02786820701376391.

Janssen, N., M. Gerlofs-Nijland, T. Lanki, R. Salonen, F. Cassee, G. Hoek, P. Fischer, B. Brunekreef, and M. Krzyzanowski (2012), Health effects of black carbon, *Res. Rep.*, World Health Organization, Regional Office for Europe, Copenhagen, Denmark.

Keller, S., and J. Heintzenberg (1997), Quantification of graphitic carbon on polycarbonate filters by Raman spectroscopy, *J. Aerosol Sci.*, *28*, suppl. 1, 609–610, doi:10.1016/S0021-8502(97)85304-9.

Khalizov, A. F., R. Zhang, D. Zhang, H. Xue, J. Pagels, and P. H. McMurry (2009), Formation of highly hygroscopic soot aerosols upon internal mixing with sulfuric acid vapor, *J. Geophys. Res.*, *114*, D05208, doi:10.1029/2008JD010595.

Knox, A., G. Evans, J. Brook, X. Yao, C. Jeong, K. Godri, K. Sabaliauskas, and J. Slowik (2009), Mass absorption cross-section of ambient black carbon aerosol in relation to chemical age, *Aerosol Sci. Technol.*, *43*(6), 522–532, doi:10.1080/02786820902777207.

Kondo, Y., et al. (2009), Stabilization of the mass absorption cross section of black carbon for filter-based absorption photometry by the use of a heated inlet, *Aerosol Sci. Technol.*, *43*(8), 741–756, doi:10.1080/02786820902889879.

Mayol-Bracero, O. L., R. Gabriel, M. O. Andreae, T. W. Kirchstetter, T. Novakov, J. Ogren, P. Sheridan, and D. G. Streets (2002), Carbonaceous aerosols over the Indian Ocean during the Indian Ocean Experiment (INDOEX): Chemical characterization, optical properties, and probable sources, *J. Geophys. Res.*, *107*(D19), 8030, doi:10.1029/2000JD000039.

Mertes, S., B. Dippel, and A. Schwarzenböck (2004), Quantification of graphitic carbon in atmospheric aerosol particles by Raman spectroscopy

and first application for the determination of mass absorption efficiencies, *J. Aerosol Sci.*, *35*(3), 347–361, doi:10.1016/j.jaerosci.2003.10.002.

Miyazaki, Y., Y. Kondo, L. Sahu, J. Imaru, N. Fukushima, and M. Kano (2008), Performance of a newly designed continuous soot monitoring system (COSMOS), *J. Environ. Monit.*, *10*(10), 1195–1201, doi:10.1039/B806957C.

Monteiro-Riviere, N., and A. Inman (2006), Challenges for assessing carbon nanomaterial toxicity to the skin, *Carbon*, *44*(6), 1070–1078.

Moosmüller, H., W. P. Arnott, C. F. Rogers, J. C. Chow, C. A. Frazier, L. E. Sherman, and D. L. Dietrich (1998), Photoacoustic and filter measurements related to aerosol light absorption during the Northern Front Range Air Quality Study (Colorado 1996/1997), *J. Geophys. Res.*, *103*(D21), 28,149–28,157, doi:10.1029/98JD02618.

Moosmüller, H., R. Chakrabarty, and W. Arnott (2009), Aerosol light absorption and its measurement: A review, *J. Quant. Spectrosc. Radiat. Transfer*, *110*(11), 844–878.

Müller, T., A. Schladitz, A. Massling, N. Kaaden, K. Kandler, and A. Wiedensohler (2009a), Spectral absorption coefficients and imaginary parts of refractive indices of Saharan dust during SAMUM-1, *Tellus B*, *61*(1), 79–95, doi:10.1111/j.1600-0889.2008.00399.x.

Müller, T., A. Schladitz, A. Massling, N. Kaaden, K. Kandler, and A. Wiedensohler (2009b), Spectral absorption coefficients and imaginary parts of refractive indices of Saharan dust during SAMUM-1, *Tellus B*, *61*(1), 79–95.

Müller, T., et al. (2011), Characterization and intercomparison of aerosol absorption photometers: Result of two intercomparison workshops, *Atmos. Meas. Tech.*, *4*(2), 245–268, doi:10.5194/amt-4-245-2011.

Naoe, H., S. Hasegawa, J. Heintzenberg, K. Okada, A. Uchiyama, Y. Zaizen, E. Kobayashi, and A. Yamazaki (2009), State of mixture of atmospheric submicrometer black carbon particles and its effect on particulate light absorption, *Atmos. Environ.*, *43*(6), 1296–1301, doi:10.1016/j.atmosenv.2008.11.031.

Neusüss, C., M. Pelzing, A. Plewka, and H. Herrmann (2000), A new analytical approach for size-resolved speciation of organic compounds in atmospheric aerosol particles: Methods and first results, *J. Geophys. Res.*, *105*(D4), 4513–4527, doi:10.1029/1999JD901038.

Nordmann, S., et al. (2009), Atmospheric aerosol measurements in the German Ultrafine Aerosol Network (GUAN) - Part 2: Comparison of measurements techniques for graphitic, light-absorbing, and elemental carbon, and the non-volatile particle volume under field conditions, *Gefahrst. Reinh. Luft*, *69*(11-12), 469–474.

Novakov, T., C. Corrigan, J. Penner, C. Chuang, O. Rosario, and O. Bracero (1997), Organic aerosols in the Caribbean trade winds: A natural source?, *J. Geophys. Res.*, *102*(D17), 21,307–21,313, doi:10.1029/97JD01487.

Petzold, A., and M. Schönlinner (2004), Multi-angle absorption photometry—A new method for the measurement of aerosol light absorption and atmospheric black carbon, *J. Aerosol Sci.*, *35*(4), 421–441, doi:10.1016/j.jaerosci.2003.09.005.

Petzold, A., et al. (2009), Saharan dust absorption and refractive index from aircraft-based observations during SAMUM 2006, *Tellus B*, *61*(1), 118–130, doi:10.1111/j.1600-0889.2008.00383.x.

Ram, K., M. Sarin, and P. Hegde (2010), Long-term record of aerosol optical properties and chemical composition from a high-altitude site (Manora Peak) in Central Himalaya, *Atmos. Chem. Phys.*, *10*(23), 11,791–11,803, doi:10.5194/acp-10-11791-2010.

Ramanathan, V., and G. Carmichael (2008), Global and regional climate changes due to black carbon, *Nat. Geosci.*, *1*(4), 221–227, doi:10.1038/ngeo156.

Rose, D., B. Wehner, M. Ketzel, C. Engler, J. Voigtländer, T. Tuch, and A. Wiedensohler (2006), Atmospheric number size distributions of soot particles and estimation of emission factors, *Atmos. Chem. Phys.*, *6*(4), 1021–1031, doi:10.5194/acp-6-1021-2006.

Rosen, H., and T. Novakov (1977), Raman scattering and the characterisation of atmospheric aerosol particles, *Nature*, *266*, 708–710, doi:10.1038/266708a0.

Sadezky, A., H. Muckenhuber, H. Grothe, R. Niessner, and U. Pöschl (2005), Raman microspectroscopy of soot and related carbonaceous materials: Spectral analysis and structural information, *Carbon*, *43*(8), 1731–1742, doi:10.1016/j.carbon.2005.02.018.

Sciare, J., H. Bardouki, C. Moulin, and N. Mihalopoulos (2003), Aerosol sources and their contribution to the chemical composition of aerosols in the Eastern Mediterranean Sea during summertime, *Atmos. Chem. Phys.*, *3*(1), 291–302, doi:10.5194/acp-3-291-2003.

Shiraiwa, M., Y. Kondo, N. Moteki, N. Takegawa, Y. Miyazaki, and D. R. Blake (2007), Evolution of mixing state of black carbon in polluted air from Tokyo, *Geophys. Res. Lett.*, *34*, L16803, doi:10.1029/2007GL029819.

Shiraiwa, M., Y. Kondo, T. Iwamoto, and K. Kita (2010), Amplification of light absorption of black carbon by organic coating, *Aerosol Sci. Technol.*, *44*(1), 46–54, doi:10.1080/02786820903357686.

Sun, H., L. Biedermann, and T. C. Bond (2007), Color of brown carbon: A model for ultraviolet and visible light absorption by organic carbon aerosol, *Geophys. Res. Lett.*, *34*, L17813, doi:10.1029/2007GL029797.

ten Brink, H., et al. (2004), INTERCOMP2000: The comparability of methods in use in Europe for measuring the carbon content of aerosol, *Atmos. Environ.*, *38*(38), 6507–6519, doi:10.1016/j.atmosenv.2004.08.027.

VDI (1996), VDI 2465 Part 1: Measurement of soot (emmission) chemical analysis of elemental carbon by extraction and thermal desorption of organic carbon, VDI/DIN-Handbuch Reinhaltung der Luft.

VDI (1999), VDI 2465 Part 2: Measurement of soot (ambient air), thermographic determination of elemental carbon after thermal desorption of organic carbon, VDI/DIN-Handbuch Reinhaltung der Luft.

Virkkula, A., N. Ahlquist, D. Covert, W. Arnott, P. Sheridan, P. Quinn, and D. Coffman (2005), Modification, calibration and a field test of an instrument for measuring light absorption by particles, *Aerosol Sci. Technol.*, *39*(1), 68–83, doi:10.1080/027868290901963.